12. Bernfield, M. R., Banerjee, S. D. & Cohn, R. H. Dependence of salivary epithelial morphology and branching morphogenesis upon acid mucopolysaccharide-protein (proteoglycan) at the epithelial surface. *J. Cell Biol.* **52,** 674–689 (1972).
13. Kadoya, Y. *et al.* Antibodies against domain E3 of laminin-1 and integrin α_6 subunit perturb branching epithelial morphogenesis of submandibular gland, but by different modes. *J. Cell Biol.* **129,** 521–534 (1995).
14. Hay, E. D. *Cell Biology of Extracellular Matrix* (Plenum, New York, 1991).
15. Nakanishi, Y., Nogawa, H., Hashimoto, Y., Kishi, J. & Hayakawa, T. Accumulation of collagen III at the cleft points of developing mouse submandibular epithelium. *Development* **104,** 51–59 (1988).
16. Velling, T., Risteli, J., Wennerberg, K., Mosher, D. F. & Johansson, S. Polymerization of type I and III collagens is dependent on fibronectin and enhanced by integrins $\alpha_{11}\beta_1$ and $\alpha_2\beta_1$. *J. Biol. Chem.* **277,** 37377–37381 (2002).
17. Yamada, K. M. & Olden, K. Fibronectins—adhesive glycoproteins of cell surface and blood. *Nature* **275,** 179–184 (1978).
18. Hardman, P. & Spooner, B. S. Localization of extracellular matrix components in developing mouse salivary glands by confocal microscopy. *Anat. Rec.* **234,** 452–459 (1992).
19. Menko, A. S., Zhang, L., Schiano, F., Kreidberg, J. A. & Kukuruzinska, M. A. Regulation of cadherin junctions during mouse submandibular gland development. *Dev. Dyn.* **224,** 321–333 (2002).
20. Elbashir, S. M., Harborth, J., Weber, K. & Tuschl, T. Analysis of gene function in somatic mammalian cells using small interfering RNAs. *Methods* **26,** 199–213 (2002).
21. Nakanishi, Y., Sugiura, F., Kishi, J. & Hayakawa, T. Collagenase inhibitor stimulates cleft formation during early morphogenesis of mouse salivary gland. *Dev. Biol.* **113,** 201–206 (1986).
22. Kashimata, M. *et al.* The ERK-1/2 signaling pathway is involved in the stimulation of branching morphogenesis of fetal mouse submandibular glands by EGF. *Dev. Biol.* **220,** 183–196 (2000).
23. Roman, J. Fibronectin and fibronectin receptors in lung development. *Exp. Lung Res.* **23,** 147–159 (1997).
24. Jiang, S. T., Chuang, W. J. & Tang, M. J. Role of fibronectin deposition in branching morphogenesis of Madin–Darby canine kidney cells. *Kidney Int.* **57,** 1860–1867 (2000).
25. Shirasuna, K., Sato, M. & Miyazaki, T. A neoplastic epithelial duct cell line established from an irradiated human salivary gland. *Cancer* **48,** 745–752 (1981).
26. Levenberg, S., Katz, B. Z., Yamada, K. M. & Geiger, B. Long-range and selective autoregulation of cell–cell or cell–matrix adhesions by cadherin or integrin ligands. *J. Cell Sci.* **111,** 347–357 (1998).
27. Grobstein, C. & Cohen, J. Collagenase: Effect on the morphogenesis of embryonic salivary epithelium *in vitro*. *Science* **150,** 626–628 (1965).
28. Sakai, T., Larsen, M. & Yamada, K. M. *Current Protocols in Cell Biology* (eds Bonifacino, J. S. *et al.*)19.3.1–19.3.30 (Wiley, New York, 2002).
29. Cukierman, E., Pankov, R., Stevens, D. R. & Yamada, K. M. Taking cell–matrix adhesions to the third dimension. *Science* **294,** 1708–1712 (2001).
30. Miekka, S. I., Ingham, K. C. & Menache, D. Rapid methods for isolation of human plasma fibronectin. *Thromb. Res.* **27,** 1–14 (1982).

Supplementary Information accompanies the paper on **www.nature.com/nature**.

Acknowledgements T.S., M.L. and K.M.Y conceived and performed the experiments; T.S. and M.L. designed the data analysis and T.S. performed it; T.S. and K.M.Y. co-wrote the paper. We thank M. P. Hoffman and R. Pankov for advice. T.S. was supported by a fellowship from the Japan Society for the Promotion of Science, and M.L. was supported by a fellowship from the NIH.

Competing interests statement The authors declare that they have no competing financial interests.

Correspondence and requests for materials should be addressed to K.M.Y. (kenneth.yamada@nih.gov).

Regulation of flowering time by light quality

Pablo D. Cerdán & Joanne Chory

Howard Hughes Medical Institute and Plant Biology Laboratory, The Salk Institute for Biological Studies, La Jolla, California 92037, USA

The transition to flowering in plants is regulated by environmental factors such as temperature and light[1]. Plants grown under dense canopies or at high density perceive a decrease in the ratio of red to far-red incoming light. This change in light quality serves as a warning of competition, triggering a series of responses known collectively as the 'shade-avoidance syndrome'. During shade avoidance, stems elongate at the expense of leaf expansion, and flowering is accelerated[2,3]. Of the five phytochromes—a family of red/far-red light photoreceptors—in *Arabidopsis*, phytochrome B (phyB) has the most significant role in shade-avoidance responses[4,5], but the mechanisms by which phyB regulates flowering in response to altered ratios of red to far-red light are largely unknown. Here we identify PFT1 (PHYTOCHROME AND FLOWERING TIME 1), a nuclear protein that acts in a phyB pathway and induces flowering in response to suboptimal light conditions. PFT1 functions downstream of phyB to regulate the expression of *FLOWERING LOCUS T* (*FT*), providing evidence for the existence of a light-quality pathway that regulates flowering time in plants.

The phytochromes and the blue/ultraviolet-A photoreceptors called cryptochromes (cry1 and cry2 in *Arabidopsis*) are critical photoreceptors that regulate seedling emergence and floral induction[6,7]. Several components involved in phytochrome signalling in seedlings have been isolated and characterized in recent years[7]. Seedlings defective in phyA signalling are tall under far-red light (FR), whereas those defective in phyB signalling are tall under red light (R). Later in development, light perceived by phyA and cry2 generates a signal that is required by CO (CONSTANS) to activate *FT*, a mechanism essential for day-length discrimination[8]. Despite the large number of phytochrome components identified, the mechanisms by which phytochromes regulate seedling development and flowering time are still largely unknown[7,9]. To identify components involved in phytochrome regulation of flowering time in *Arabidopsis*, we devised a new genetic screen (see Methods). Seedlings showing an enhanced response to pulses of red light were selected and transplanted to soil and then scored for defects in flowering time. One of the recessive mutants, *pft1*, is characterized in detail here.

Consistent with a role in phytochrome signalling, *pft1* mutants displayed small but significant effects on hypocotyl-length inhibition under both red and far-red light (Fig. 1a). The mutants were hypo-responsive to far-red and hyper-responsive to red. These altered responses to light required functional phyA and phyB (Fig. 1a). The levels of phyA and phyB protein were unaltered in *pft1* compared with wild type, suggesting that PFT1 affects processes downstream of phyA and phyB (data not shown). Negative effects of phyA signalling on phyB signalling, as well as negative effects of phyB on phyA function, have been reported previously[10,11]. The *pft1* mutation has opposite effects on phyA- and phyB-mediated responses, indicating that PFT1 may function in phytochrome signalling at a node where antagonistic interactions occur between phyA and phyB. The *pft1* mutants had normal responses to blue light (data not shown), suggesting that PFT1 is specific for phytochrome action and is not a general regulator of light responsiveness.

pft1 mutants displayed a late-flowering phenotype when grown under long-day conditions (LD, 16 h light/8 h dark; Fig. 1b, c). phyA and phyB regulate flowering time in opposing ways: phyB acts to delay flowering under both long- and short-day (SD, 9 h light/15 h dark) conditions, whereas phyA weakly promotes flowering in long days[6]. We measured flowering time under both LD and SD conditions in *pft1*, *pft1 phyB*, *pft1 phyA* and *pft1 phyA phyB* mutants, and compared the results with *phyB*, *phyA* and *phyA phyB* mutants (Fig. 1c, d). *pft1* was late flowering and completely suppressed the early-flowering phenotype of *phyB* in both LD and SD conditions, strongly suggesting that PFT1 is essential for phyB regulation of flowering time. The effects of *pft1* on the photoperiodic induction of flowering were relatively minor in both wild-type and in phytochrome mutant backgrounds (Fig. 1c, d), indicating that PFT1 is unlikely to act in the photoperiod pathway that induces flowering.

PFT1 may also act downstream of phyA, as the effects of *phyA* and *pft1* mutations in delaying flowering under LD were not additive. However, a phyA-dependent photoperiod response is still present in the absence of PFT1 or phyB, because *pft1 phyA phyB* mutants flowered significantly later than *pft1 phyB* mutants under LD but not SD. It has been proposed[12] that phyA can promote flowering by two independent mechanisms: by suppressing phyB function, and independently of phyB. Our data are consistent with this report, and they suggest that the effects of *pft1* on phyA regulation of flowering

time may be an indirect effect of changes in the phyB pathway.

The increased petiole length of *phyB* mutants was largely unaffected in the *pft1 phyB* double mutants (Fig. 1e). These results, together with the mild effects of *pft1* on hypocotyl length, the strong response to photoperiod in *pft1* mutants in phytochrome-deficient backgrounds and the complete suppression of *phyB*'s early-flowering phenotype suggest that the main role of PFT1 in phytochrome signalling is to regulate flowering time downstream of phyB in a photoperiod-independent pathway.

Cloning of *PFT1* revealed that it encodes a putative protein of 836 amino acids, with a predicted vWF-A (von Willebrand factor type A) domain in the amino terminus[13,14] and a glutamine-rich region in the carboxy terminus, reminiscent of some transcriptional activators[15] (Fig. 2a). vWF-A domains are widely distributed among all phyla[14]. They are involved in various cellular processes, and a high proportion have a divalent cation-binding site that in some cases has been shown to mediate protein–protein interactions[16]. The DxSxS motif involved in coordination with a divalent cation is converted to ExTxA in PFT1. It is unclear whether this partially conserved motif in PFT1 can still bind a metal.

The *pft1* mutant produced a truncated messenger RNA (Fig. 2b), and transformation with a genomic copy of *PFT1* rescued both the seedling and flowering time defects (Fig. 2d–f). We found that *PFT1* is limiting for flowering under SD, as overexpression of *PFT1* caused an early-flowering phenotype under these conditions (Fig. 2f, g). This result is also consistent with the strongest effects of the *phyB* mutation observed under SD (Fig. 1c, d). Transformation of *pft1* plants with *PFT1* complementary DNA under the strong 35S promoter also produced a high proportion of co-suppressed plants whose phenotypes were not more severe than the *pft1* mutant. These data support the interpretation that the *pft1* allele is a strong or null allele (Fig. 2f, g and data not shown).

To study the subcellular localization of PFT1, we fused the gene encoding green fluorescent protein (GFP) to either the N or the C terminus of *PFT1* in the context of the genomic clone. These constructs encoded a functional protein, as they complemented the *pft1* phenotype (data not shown). Both N- and C-terminal GFP fusions localized to the nucleus (Fig. 2c and data not shown). The subcellular location of PFT1–GFP did not change in response to red, far-red or white light (data not shown). These observations, together with the mild effect of the *phyB* mutation on *PFT1* mRNA levels (see Supplementary Information), indicate that phyB regulation of *PFT1* activity occurs post-transcriptionally or through association with other proteins.

The glutamine-rich region of PFT1 (Fig. 2a), its nuclear localization (Fig. 2c) and its ability to activate transcription in yeast when fused to the LexA DNA-binding domain (data not shown) suggested that PFT1 might function as a transcriptional co-activator. To test the nature of *phyB* suppression by *pft1*, we investigated its role in the regulation of key genes that affect flowering time. *FT* is an

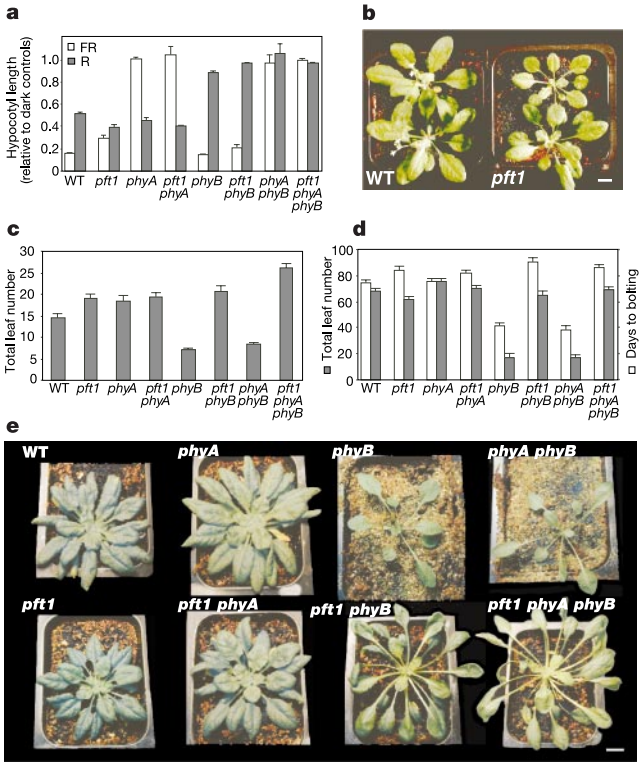

Figure 1 Phenotypes of *pft1*, *phyA* and *phyB* single, double and triple mutants. **a**, Hypocotyl length of 5-day-old seedlings of the indicated genotypes grown for 4 days under 3 μmol m^{-2} s^{-1} of far-red light (FR) or 10 μmol m^{-2} s^{-1} of red light (R). **b**, Wild-type (WT) and *pft1* plants grown as described in **c**. **c**, **d**, Flowering time of the indicated genotypes grown under long-day (16 h white light; 8 h dark; **c**) and short-day (9 h white light; 15 h dark; **d**) conditions. **e**, The genotypes used in **a**, **c** and **d**, cultivated in short days for 5 (*phyB* and *phyA phyB*) or 9 (WT, *pft1*, *phyA*, *pft1 phyA*, *pft1 phyB* and *pft1 phyA phyB*) weeks. Note that in *phyB* and *phyA phyB*, the apical meristem is already converted to an inflorescence meristem, whereas no sign of change is observed in the *pft1* background. Data represent averages of three independent experiments (**a**) and eight to ten plants (**c**, **d**) ±s.e. Scale bar, 1 cm.

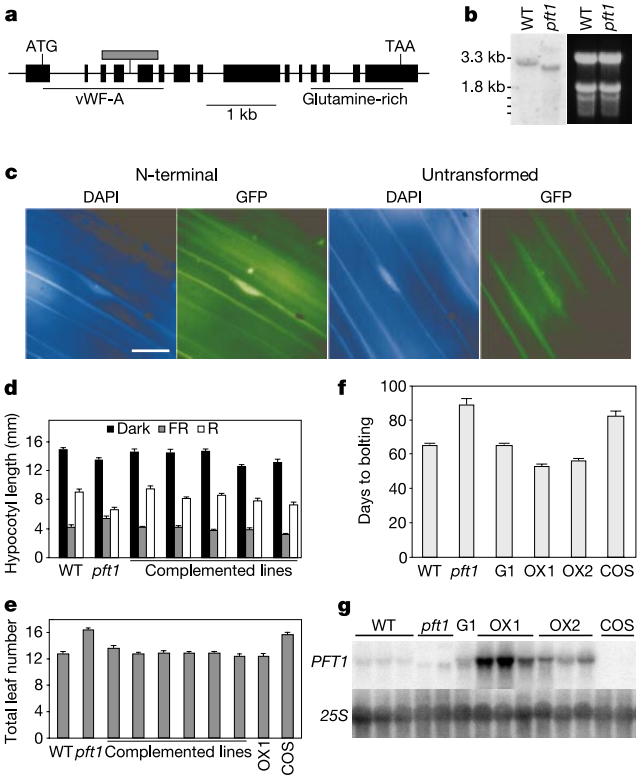

Figure 2 Molecular characterization of *PFT1*. **a**, Structure of the *PFT1* gene. Black boxes represent exons; lines represent introns. Predicted domains and the T-DNA insertion (out of scale) are indicated. Scale bar, 1 kb. **b**, Northern blot of WT and *pft1* (left) and the corresponding gel (right). **c**, Localization of GFP–PFT1 fusions and the corresponding controls, 4,6-diamidino-2-phenylindole (DAPI) staining and non-transgenic lines, as indicated. Scale bar, 10 μm. **d**, **e**, **f**, Molecular complementation of the hypocotyl-length phenotype (**d**), late-flowering phenotype in long days (**e**) and delayed bolting in short days (**f**). Different transgenic lines for the *PFT1* gene were used, as indicated. OX1 and OX2 are 35S–PFT1-overexpressing lines in *pft1* and WT backgrounds, respectively. COS is a co-suppressed line in *pft1* background, and G1 is a complemented line. **g**, *PFT1* mRNA levels and the corresponding ribosomal RNA control for the lines shown in **f**.

integrator of several flowering time pathways[8,17–19]. *FT* expression is lower in *phyA* and *cry2* mutants in conditions where these mutants are late flowering[8]. We analysed the expression patterns of *FT* mRNA in wild-type, *phyB*, *pft1* and *phyB pft1* double mutants. We first tested expression levels in 8-day-old seedlings, as previously described[8,20,21]. In LD-grown seedlings, *FT* expression was substantially higher in *phyB* mutants than in wild type (Fig. 3a, b), indicating that phyA and phyB have opposing roles in flowering by differentially regulating *FT* expression. By contrast, these differences were not found in 8-day-old seedlings grown in SD, consistent with previous reports[21] (data not shown). This could be due to the lack of commitment to flowering of SD-grown seedlings at this early stage of development (wild-type plants produce about 70 leaves in SD conditions, whereas primary leaves are just emerging in 8-day-old seedlings). Thus, we tested *FT* mRNA levels in 26-day-old plants grown in SD, a time at which *phyB* mutants are roughly two weeks from showing visible floral buds. Under these conditions, we observed a large increase in *FT* mRNA levels in *phyB* mutants compared with wild-type plants (Fig. 3c, d). These data thus provide a molecular mechanism for the early flowering time of *phyB* mutants in both LD and SD. Moreover, *FT* mRNA levels were low in *pft1* and *pft1 phyB* double mutants in all the conditions tested (Fig. 3a–d), pointing to the molecular mechanism for the suppression of the early-flowering-time phenotype of *phyB* mutants by *pft1*.

CO is a key component[22] of the photoperiod pathway, which integrates information from the circadian clock[20] as well as phyA and cry2 signalling[8]. CO also directly activates *FT* expression[23]. We found higher levels of *CO* mRNA in LD-grown *phyB* seedlings than in wild type, and lower levels in the *pft1* background, suggesting that PFT1 might function upstream of CO in the regulation of *FT* (Fig. 3a, b). However, in SD-grown plants, we were unable to detect increased levels of *CO* in *phyB* mutants, nor were the levels decreased in the *pft1* background (Fig. 3c, d). We extended this analysis to *SOC1*, another floral integrator[24,25], and did not observe a correlation of *SOC1* mRNA levels with flowering time, in either *phyB* or *pft1* mutant backgrounds (see supplement to Fig. 3 in Supplementary Information). The lack of a significant correlation between *CO* and *SOC1* mRNA levels with *phyB* and *pft1* flowering times suggests that phyB regulates *FT* mRNA levels by a PFT1-dependent mechanism that does not involve changes in *CO* or *SOC1* mRNA levels. It has been suggested that light post-translationally regulates CO activity[20]. However, *pft1* does not have a significant effect on flowering time or on *FT* mRNA levels in a *CO*-overexpressing line, arguing that PFT1 does not have a significant role in the post-translational regulation of CO (Fig. 4a and data not shown).

If PFT1 has a specific role in a phyB pathway that regulates flowering time in response to changes in light quality, then *pft1* mutants should be unable to accelerate flowering in response to shade conditions. We grew wild-type plants and *pft1* mutants in SD

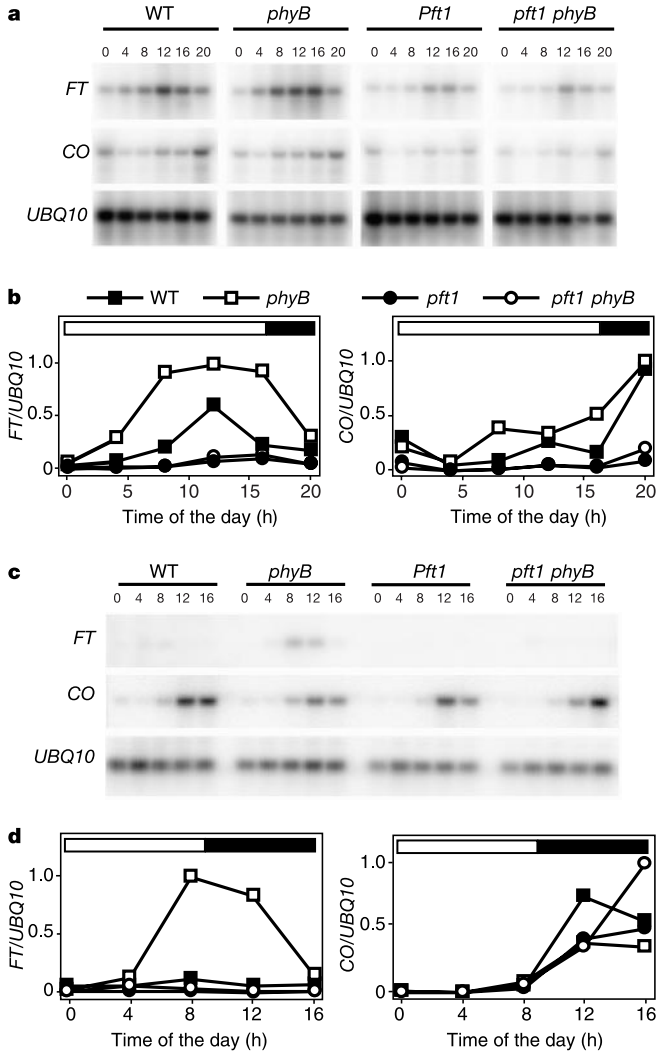

Figure 3 *FT* and *CO* mRNA levels in WT, *phyB*, *pft1* and *pft1 phyB* mutants. **a**, *FT* and *CO* expression in 8-day-old seedlings grown under long-day conditions and harvested at the indicated times. 0, lights on. **b**, Quantification of data shown in **a** relative to the *UBQ10* control. **c**, *FT* and *CO* expression in 26-day-old plants grown under short-day conditions and harvested at the indicated times. 0, lights on. **d**, Quantification of data shown in **c** relative to the *UBQ10* control. Data in **a** and **c** represent two independent experiments.

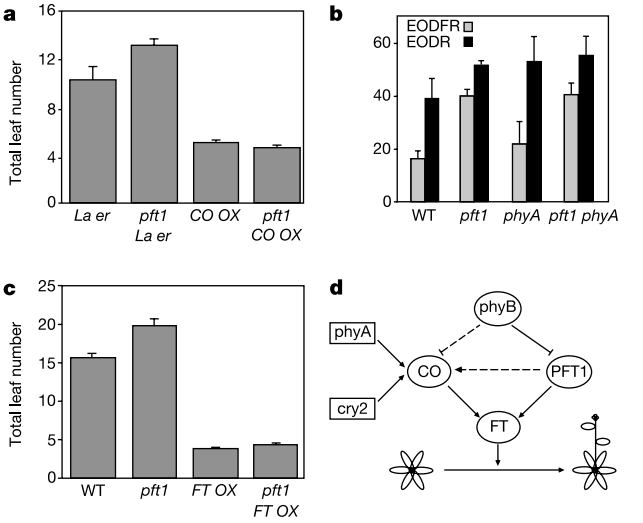

Figure 4 PFT1 acts in a light-quality pathway upstream of *FT*. **a**, Flowering time of WT (cv. *Landsberg erecta*), *pft1*, *CO* overexpresser in WT (*CO OX*) and *pft1* (*pft1 CO OX*) backgrounds. For this particular experiment the *pft1* mutation was introgressed four times into the *L. erecta* ecotype before crossing to *CO OX* lines. **b**, Flowering time of the indicated genotypes grown under short-day conditions in factorial combination with 15 min of red or far-red light at the end of each photoperiod (EODR and EODFR). Data are mean ± s.e. of seven to nine plants. **c**, Flowering time of WT, *pft1*, *FT*-overexpresser in WT (*FT OX*) and *pft1* (*pft1 FT OX*) backgrounds. Data from **a** and **c** are mean ± s.e. of at least ten plants grown under long-day conditions. **d**, A proposed model to explain PFT1 involvement in a light-quality pathway that regulates flowering time. With the exception of the direct regulation of *FT* by CO (ref. 23), other arrows do not represent direct regulation or interaction. phyA and cry2 seem to mediate a direct effect of light on CO activity[8]. The role of FT in the proposed pathway is based on previous studies[18,19]. The placement of PFT1 is deduced from the work presented here.

followed by an end-of-day pulse of far-red (EODFR) or red (EODR) light. The EODFR pulse mimics the effects of shade, including accelerated flowering. The promotion of flowering by the EODFR treatment (compared with EODR controls) was severely impaired in the *pft1* and *pft1 phyA* mutants compared with wild type and *phyA*, respectively (Fig. 4b), consistent with a role in signalling after perception of low red/far-red ratios. It is possible that PFT1 acts in an autonomous pathway, independently of changes in light quality, but we feel that this is unlikely, as *pft1* effects on flowering are mild, except in a *phyB* background, and the *pft1* mutation specifically impairs the response to low red/far-red ratios. As mentioned, it is also unlikely that PFT1 has a role in a photoperiod pathway, as *pft1* and *pft1 phyB* double mutants show a strong response to photoperiod (Fig. 1c, d), in contrast to *co* and *co phyB* double mutants[3,22,26]. This notion is reinforced by our observation that PFT1 can regulate *FT* mRNA levels by mechanisms that do not involve CO. Finally, the pattern of expression of *FT* in *phyB* and *pft1* single and double mutants indicates that the activation of *FT* occurs downstream of PFT1 in a phyB pathway, consistent with the lack of effect of the *pft1* mutation in a *FT*-overexpressing background (Fig. 4c).

A 'light-quality' pathway has been proposed[9] to explain the role of phyB and other stable phytochromes (phyD and phyE in *Arabidopsis*) in flowering. This light-quality perception pathway may be involved in the shade-avoidance syndrome triggered in response to low red/far-red ratios[2,3]. Here we present genetic and molecular evidence that this light-quality pathway exists, and we incorporate a new component, PFT1, into this signalling pathway. Our results are consistent with a model (Fig. 4d) in which PFT1 acts in a light-quality pathway downstream of phyB. The resulting signal is then integrated with the photoperiod pathway through the modulation of *FT* transcription. □

Methods

Plant material and growth conditions

Except when stated otherwise, all experiments were done in the Columbia accession. The alleles for the different mutants used were *phyA211* and *phyB9*. *FT*- and *CO*-overexpressing lines were provided by D. Weigel. Seeds were sterilized using chlorine in a vapour phase. For RNA extraction, we used total seedlings grown in MS media without sucrose, or shoots from mature plants grown on soil. For hypocotyl measurements, seedlings were grown in water–agar medium. Red and far-red light treatments were done in chambers of light-emitting diodes (Percival Scientific) at 23 °C. White light sources were always from fluorescent tubes, 40–70 $\mu mol\,m^{-2}\,s$ for LD and SD, respectively, except for incandescent light extensions (LI) with 2 $\mu mol\,m^{-2}\,s$ of photosynthetic active radiation (400–700 nm).

For the genetic screen, activation-tagged transfer DNA lines were obtained from the Arabidopsis Stock Center as pools representing around 100 lines each. These lines are at least in the T3 generation, so recessive mutations can also be found. Each pool was plated on water–agar medium, and stratified for 3 days. Germination was induced by 1 h of white light, and then seedlings received 5 min of red light every 24 h. On the fourth day, seedlings were scored for signs of de-etiolation, such as shorter hypocotyls or partially opened cotyledons, and transplanted to soil to score adult phenotypes.

Molecular characterization of *PFT1*

Genomic DNA was extracted from *pft1* mutants, cut with *Hind*III and *Eco*RI for right border rescue, and with *Bam*HI and *Spe*I for left border rescue, and ligated and electroporated into SURE competent cells (Stratagene). Genomic DNA was successfully rescued with *Hind*III, *Bam*HI and *Spe*I restriction enzymes. We designed specific oligonucleotides to detect by polymerase chain reaction (PCR) the T-DNA insertion in hemizygous and homozygous lines. The following three primers were used in PCR: 5′-CAGAGGAACCCTGTTTCTACTGTTGAGCT-3′, 5′-CGTTACTTGGTTGAGCTTGGCCTGAAGGA-3′ and 5′-TCCCGGACATGAAGCCATTTATATGTA-3′. The expected PCR products were 563 base pairs (bp) for the wild type and 491 bp for the mutant, and both bands were detected in hemizygotes.

The T-DNA co-segregated with the *pft1* mutation in 140 chromosomes analysed. We also tested 36 F3 populations and noted that the Basta resistance (conferred by the T-DNA) also co-segregated with the *pft1* mutation. Southern blot data and the rescued genomic DNA sequence agreed with a single insertion on BAC F2J7 from chromosome I.

Intron–exon junctions were derived by comparison with EST clone APZL03h11R (GenBank accession number AV528220). To confirm the 5′ end, RACE (rapid amplification of cDNA ends)–PCR was performed using the GeneRacer kit according to the manufacturer's instructions (Invitrogen). In *pft1* mutants, an mRNA species of lower molecular weight was observed (Fig. 3b). We used RACE–PCR to characterize this form further, and found that it corresponds to a 2.5-kilobase (kb) truncated form of *PFT1* that initiates within the T-DNA.

The genomic *PFT1* clone was subcloned from BAC F2J7 in two consecutive steps into binary plasmid pPZP212, finally as a *Pst*I–*Sac*I 8.5-kb fragment and introduced into *pft1* mutants by transformation with *Agrobacterium tumefaciens*. Transgenic lines were selected on MS media supplemented with 50 $\mu g\,ml^{-1}$ of kanamycin, screened for single-locus insertions in the T2 generation, and the homozygous lines from the T3 generation used for physiological experiments.

To make the GFP fusion proteins, *Eco*RI sites were introduced in-frame right before the ATG start codon (for GFP–PFT1 fusions) and right before the TAA stop codon (for PFT1–GFP fusions). The GFP-coding region amplified by PCR was subcloned into these *Eco*RI sites, and final constructs were confirmed by sequencing before being used for plant transformation as described above.

To assess a phenotype of overexpression, the *PFT1* cDNA was subcloned in two steps as a *Bam*HI–*Pst*I–*Pst*I fragment into CHF1 and CHF3 plasmids under the 35S constitutive promoter. After plant transformation, lines were selected on kanamycin (CHF3-derived plasmids) or gentamycin (70 $\mu g\,ml^{-1}$ CHF1-derived plasmids).

mRNA quantification

Specific mRNAs were extracted and quantified by RT–PCR (PCR with reverse transcription), essentially as described[21]. mRNA was reverse transcribed using the 1st cDNA synthesis kit according to the manufacturer's instructions (Invitrogen). Primers, annealing temperatures and the size of PCR products expected were as follows: *FT*, 5′-GCTACAACTGGAACAACCTTTGGCAAT-3′, 5′-TATAGGCATCATCACCGTTCGTTACTC-3′, 63 °C, 365 bp; *CO*, 5′-AAACTCTTTCAGCTCCATGACCACTACT-3′, 5′-CCATGGATGAAATGTATGCGTTATGGTTA-3′, 62 °C, 453 bp; *UBQ10*, 5′-GGTGTCAGAACTCTCCACCTCAAGAGTA-3′, 5′-TCAATTCTCTCTACCGTGATCAAGATGCA-3′, 64 °C, 318 bp; *TSF*, 5′-GAAATTTCTACACCTTGGTTATGGTGGA-3′, 5′-CTTTACATCGATGTCAGCATATGCATCA-3′, 63 °C, 484 bp. In all cases, at least one of the primers used for PCR spanned intron–exon junctions, and amplification of genomic DNA was undetectable in non-retrotranscribed controls. *SOCI*/*AGL20* was quantified by RT–PCR, as described[27]. PCR products were detected by Southern blot using standard methodology, and quantified using a Phosphorimager (Molecular Dynamics) in the exponential range of amplification.

Received 31 October 2002; accepted 14 April 2003; doi:10.1038/nature01636.

1. Levy, Y. Y. & Dean, C. Control of flowering time. *Curr. Opin. Plant Biol.* **1,** 49–54 (1998).
2. Ballare, C. L. Keeping up with the neighbours: phytochrome sensing and other signalling mechanisms. *Trends Plant Sci.* **4,** 201 (1999).
3. Halliday, K. J., Koornneef, M. & Whitelam, G. C. Phytochrome B and at least one other phytochrome mediate the accelerated flowering response of *Arabidopsis thaliana* L. to low red/far-red ratio. *Plant Physiol.* **104,** 1311–1315 (1994).
4. Aukerman, M. J. *et al.* A deletion in the *PHYD* gene of the *Arabidopsis* Wassilewskija ecotype defines a role for phytochrome D in red/far-red light sensing. *Plant Cell* **9,** 1317–1326 (1997).
5. Devlin, P. F., Patel, S. R. & Whitelam, G. C. Phytochrome E influences internode elongation and flowering time in *Arabidopsis*. *Plant Cell* **10,** 1479–1487 (1998).
6. Lin, C. Photoreceptors and regulation of flowering time. *Plant Physiol.* **123,** 39–50 (2000).
7. Quail, P. H. Phytochrome photosensory signalling networks. *Nature. Rev. Mol. Cell Biol.* **3,** 85–93 (2002).
8. Yanovsky, M. J. & Kay, S. A. Molecular basis of seasonal time measurement in *Arabidopsis*. *Nature* **419,** 308–312 (2002).
9. Simpson, G. G. & Dean, C. *Arabidopsis*, the Rosetta stone of flowering time? *Science* **296,** 285–289 (2002).
10. Cerdan, P. D. *et al.* Regulation of phytochrome B signaling by phytochrome A and FHY1 in *Arabidopsis thaliana*. *Plant J.* **18,** 499–507 (1999).
11. Hennig, L., Poppe, C., Sweere, U., Martin, A. & Schafer, E. Negative interference of endogenous phytochrome B with phytochrome A function in *Arabidopsis*. *Plant Physiol.* **125,** 1036–1044 (2001).
12. Mockler, T. *et al.* Regulation of photoperiodic flowering by *Arabidopsis* photoreceptors. *Proc. Natl Acad. Sci. USA* **100,** 2140–2145 (2003).
13. Ponting, C. P., Schultz, J., Milpetz, F. & Bork, P. SMART: identification and annotation of domains from signalling and extracellular protein sequences. *Nucleic Acids Res.* **27,** 229–232 (1999).
14. Ponting, C. P., Aravind, L., Schultz, J., Bork, P. & Koonin, E. V. Eukaryotic signalling domain homologues in archaea and bacteria. Ancient ancestry and horizontal gene transfer. *J. Mol. Biol.* **289,** 729–745 (1999).
15. Escher, D., Bodmer-Glavas, M., Barberis, A. & Schaffner, W. Conservation of glutamine-rich transactivation function between yeast and humans. *Mol. Cell. Biol.* **20,** 2774–2782 (2000).
16. Hinshelwood, J. & Perkins, S. J. Metal-dependent conformational changes in a recombinant vWF-A domain from human factor B: a solution study by circular dichroism, fourier transform infrared and ^{1}H NMR spectroscopy. *J. Mol. Biol.* **298,** 135–147 (2000).
17. Levy, Y. Y., Mesnage, S., Mylne, J. S., Gendall, A. R. & Dean, C. Multiple roles of *Arabidopsis VRN1* in vernalization and flowering time control. *Science* **297,** 243–246 (2002).
18. Kardailsky, I. *et al.* Activation tagging of the floral inducer *FT*. *Science* **286,** 1962–1965 (1999).
19. Kobayashi, Y., Kaya, H., Goto, K., Iwabuchi, M. & Araki, T. A pair of related genes with antagonistic roles in mediating flowering signals. *Science* **286,** 1960–1962 (1999).
20. Suarez-Lopez, P. *et al.* *CONSTANS* mediates between the circadian clock and the control of flowering in *Arabidopsis*. *Nature* **410,** 1116–1120 (2001).
21. Blazquez, M. A. & Weigel, D. Independent regulation of flowering by phytochrome B and gibberellins in *Arabidopsis*. *Plant Physiol.* **120,** 1025–1032 (1999).
22. Putterill, J., Robson, F., Lee, K., Simon, R. & Coupland, G. The *CONSTANS* gene of *Arabidopsis* promotes flowering and encodes a protein showing similarities to zinc finger transcription factors. *Cell* **80,** 847–857 (1995).
23. Samach, A. *et al.* Distinct roles of *CONSTANS* target genes in reproductive development of *Arabidopsis*. *Science* **288,** 1613–1616 (2000).
24. Hepworth, S. R., Valverde, F., Ravenscroft, D., Mouradov, A. & Coupland, G. Antagonistic regulation

of flowering-time gene SOC1 by CONSTANS and FLC via separate promoter motifs. *EMBO J.* **21,** 4327–4337 (2002).
25. Lee, H. *et al.* The AGAMOUS-LIKE 20 MADS domain protein integrates floral inductive pathways in *Arabidopsis*. *Genes Dev.* **14,** 2366–2376 (2000).
26. Koornneef, M., Hanhart, C., Van Loenen-Martinet, P. & Blankestijn-de Vries, H. The effect of daylength on the transition to flowering in phytochrome-deficient, late-flowering and double mutants of *Arabidopsis thaliana*. *Physiol. Plant* **95,** 260–266 (1995).
27. Blazquez, M. A., Trenor, M. & Weigel, D. Independent control of gibberellin biosynthesis and flowering time by the circadian clock in *Arabidopsis*. *Plant Physiol.* **130,** 1770–1775 (2002).

Supplementary Information accompanies the paper on **www.nature.com/nature**.

Acknowledgements We thank the Kasuza Research Institute and the *Arabidopsis* Stock Center for providing EST clone APZL03h11R and BAC F2J7, respectively; D. Weigel for providing *FT*- and *CO*-overexpressing lines, and for useful advice; P. Wigge, S. Mora-Garcia, D. Weigel, J. Nemhauser, M. Yanovsky and J. Casal for comments on the manuscript; L. Barden for figure preparation; and B. Smoot, N. Ga and M. Ledgerwood for technical assistance. This work was supported by a grant from the National Institutes of Health to J.C. (GM52413) and by the Howard Hughes Medical Institute. P.C. was a fellow of the PEW Latin American Fellows Program and Fundación Antorchas.

Competing interests statement The authors declare that they have no competing financial interests.

Correspondence and requests for materials should be addressed to J.C. (chory@salk.edu). The GenBank accession code for *PFT1* is AY170377.

CUL-4 ubiquitin ligase maintains genome stability by restraining DNA-replication licensing

Weiwei Zhong, Hui Feng, Fernando E. Santiago & Edward T. Kipreos

Department of Cellular Biology, University of Georgia, Athens, Georgia 30602, USA

To maintain genome stability, DNA replication is strictly regulated to occur only once per cell cycle. In eukaryotes, the presence of 'licensing proteins' at replication origins during the G1 cell-cycle phase allows the formation of the pre-replicative complex[1]. The removal of licensing proteins from chromatin during the S phase ensures that origins fire only once per cell cycle[1]. Here we show that the CUL-4 ubiquitin ligase temporally restricts DNA-replication licensing in *Caenorhabditis elegans*. Inactivation of CUL-4 causes massive DNA re-replication, producing cells with up to 100C DNA content. The *C. elegans* orthologue of the replication-licensing factor Cdt1 (refs 2, 3) is required for DNA replication. *C. elegans* CDT-1 is present in G1-phase nuclei but disappears as cells enter S phase. In cells lacking CUL-4, CDT-1 levels fail to decrease during S phase and instead remain constant in the re-replicating cells. Removal of one genomic copy of *cdt-1* suppresses the *cul-4* re-replication phenotype. We propose that CUL-4 prevents aberrant re-initiation of DNA replication, at least in part, by facilitating the degradation of CDT-1.

CUL-4 is a member of the cullin ubiquitin-ligase family[4]. Cullins function in cullin/RING finger complexes to catalyse the covalent attachment of ubiquitin to protein substrates to mark them for proteolysis[5]. In *C. elegans*, the *cul-4* gene is expressed throughout development. In adult hermaphrodites, *cul-4* messenger RNA is observed primarily in the germ line, with transient expression in the intestine of young adults (Fig. 1a, b; data not shown). *cul-4* maternal mRNA is present in early embryos and decreases during embryogenesis (Fig. 1c, d). In larvae, *cul-4* is broadly expressed, with high levels in proliferating tissues, notably in the intestine and germ line (Fig. 1e).

To probe *cul-4* function, we used RNA-mediated interference (RNAi)[6] to inactivate the *cul-4* gene. *cul-4* RNAi reduced *cul-4* mRNA to levels not significantly higher than background (Fig. 1f–h). The predominant *cul-4* RNAi phenotype was a developmental arrest at the L2 larval stage. We observed a pronounced increase in the size of blast cell nuclei in *cul-4* RNAi L2 larvae. In a *clr-1*(*e1745*) genetic background that allows the visualization of cell boundaries[7], *cul-4* RNAi produced a marked increase in the size of seam cells (Fig. 2a, b). However, the size of nuclei in the non-proliferative hyp7 syncytial cell[8] was unaffected by inactivation of *cul-4* (Fig. 2a, b). Larger cells were also observed among other *cul-4* RNAi blast cell lineages, including the M, Q, P and somatic gonad cell lineages (Fig. 2c–f; data not shown). Germ cells did not become enlarged. However, germ cells often entered meiosis prematurely to become sperm in the L2 larval stage; this is in contrast to the wild type, in which spermatogenesis occurs in the L4 larval stage[9] (Fig. 2e, f). We assume that this premature spermatogenesis results

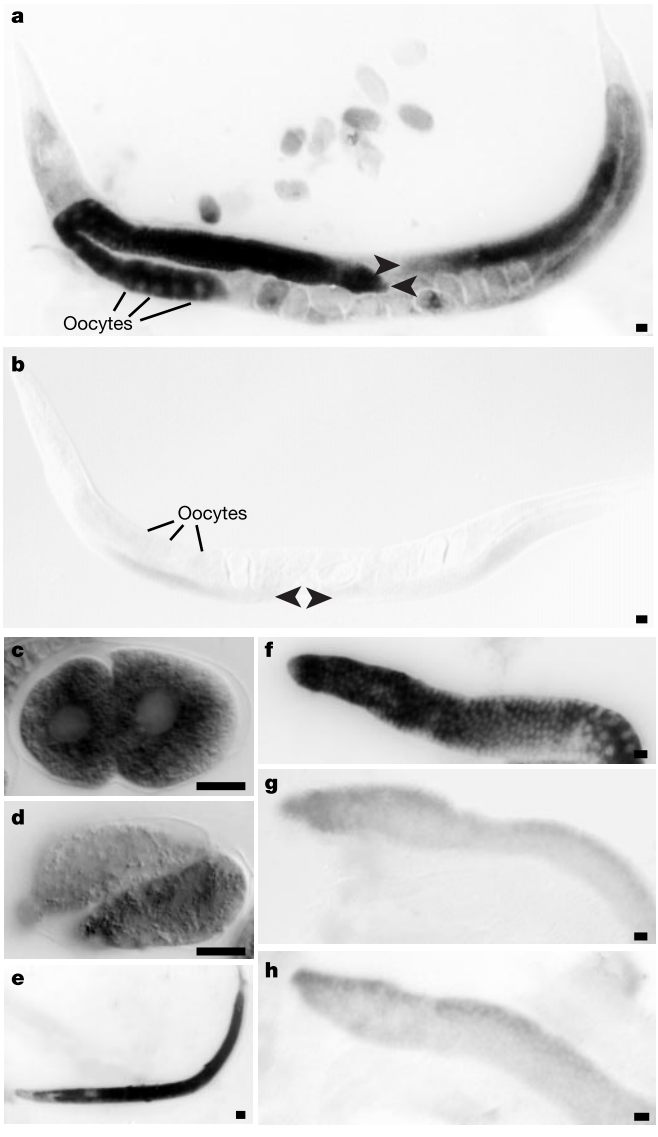

Figure 1 *cul-4* mRNA levels. **a**, **b**, *In situ* hybridization of wild-type adult hermaphrodites with *cul-4* antisense (**a**) or control sense (**b**) probes. Arrowheads mark the distal ends of the gonad arms; anterior oocytes are labelled. **c**–**e**, *In situ* hybridization with antisense *cul-4* probe of a two-cell-stage embryo (**c**), twofold-stage embryo (**d**) and L2 larva (**e**). **f**–**h**, *In situ* hybridization of dissected gonads from wild-type adult hermaphrodites (**f**, **h**) or wild-type hermaphrodite injected with *cul-4* dsRNA (**g**) probed with antisense *cul-4* (**f**, **g**) or sense *cul-4* (**h**). Scale bars, 10 μm.